Tuijin Jishu/Journal of Propulsion Technology
ISSN: 1001-4055
Vol. 46 No. 3 (2025)

Numerical analysis of heat and mass transfer in magnetohydrodynamic hybrid Nanofluid (SWCNTs + Ag + Gasoline) flow over a variable thickness sheet with melting heat effects

Narmatha M [1], Rohith Roshan A[2], Muthu Mekala N [3], Sumathi K [4,*]

[1]Department of Mathematics, KPR Institute of Engineering and Technology, Coimbatore 641 407, India.

[2,3]Department of Mechanical Engineering, Engineering design division, College of Engineering, Guindy, Chennai 600 025, India.

[4]Department of Mathematics, PSGR Krishnammal College for Women, Coimbatore 641 004, India.

Abstract: The work examines the heat and mass transfer in the melting process of a hybrid Nanofluid (SWCNTs + Ag + Gasoline) flow subject to a magnetic field over a sheet of variable thickness. Analysis incorporates multiple physical phenomena such as melting heat, viscous dissipation, magnetic field, Brownian diffusion and thermophoretic diffusion in mass concentration. Through similarity variable transformations, the PDEs are reduced to coupled ODEs. The influence of mass concentration on diffusion and heat transfer properties as well as its interplay with temperature field is examined in detail. The MHD effects are explored, highlighting the role of the magnetic field on fluid velocity, temperature and mass transfer rates. To solve the boundary value problem, the bvp4c solver of MATLAB (9.14) is employed. The analysis explores the influence of various dimensionless parameters on the flow characteristics such as velocity, temperature, concentration, wall shear stress, rate of heat and mass transfer. The results visually provide insights that are applicable to energy storage systems, industrial melting processes and magnetic cooling applications.

Keywords: Nanofluid, Hybrid nanofluid, viscous dissipation, MHD, melting heat, Brownian diffusion, Thermophoretic diffusion.

1. Introduction

In recent years, nanofluids have emerged as highly efficient materials with diverse applications in pharmaceutical, biological and industrial sectors. Choi and Eastman [1] pioneered the concept of nanofluids to demonstrate that suspending nanoparticles in base fluids significantly enhances thermal conductivity. This ground breaking work established the scientific basis for using nanofluids in heat transfer applications. Vajravelu [2] conducted foundational work analyzing viscous flow characteristics along nonlinear stretching surfaces. His theoretical studies explained how nonlinear stretching parameters influence velocity profiles and boundary layer development, providing crucial insights for industrial processes involving material stretching. Based upon these concepts Fang et. al. [3] explored the flow and heat transfer phenomena in the boundary layer over a stretched sheet exhibiting variable thickness, with an emphasis on mathematical modeling and computational analysis of how thickness change affects flow behavior. The study by Ali et al. [4] focused on magnetohydrodynamic peristaltic transport involving Jeffery material through a TiO2-Cu/H2O hybrid nanofluid considering the effects of slip conditions. Jahan et al. [5] conducted a study on the thermal and flow characteristics of nanofluids interacting with a permeable surface exhibiting nonlinear stretching or shrinking sheet using a new mathematical

model and stability analysis. Mukhopadhyay [6] studied thermal magnetohydrodynamic boundary layer flow across an exponentially stretching sheet by assessing its thermal stratification throughout the fluid. Robert [7] investigated hot air stream effects on semi-infinite ice masses during melting while identifying the relevant fluid dynamic factors involved in heat transfer. Gireesha et al. [8-9] studied stagnation point nanofluid boundary layers on stretched sheets while analyzing induced magnetic fields effects in their work. Hayat et al. [10] investigated stagnation point behavior in pair stress fluids while studying heat exchange effect on flow system. Khilap Singh and Manoj Kumar [11] studied the motion of a stagnation point boundary as it travels through a micropolar fluid adjacent to a stretched sheet while analyzing heat and melting absorption effects. Hayat et al. [12] studied how carbon nanotubes transfer melting heat when flowing toward surfaces of different thicknesses at stagnation points. Turkyilmazoglu [13] investigated natural convective nanofluid flow near a sudden vertical plate under thermal radiation conditions. Khader and Megahed [14] performed numerical simulations on boundary layer flow emerged from a nonlinear stretching sheet with variable thickness while taking into account slip velocity effects. Prasad et al. [15] studied thermal behaviour of magnetohydrodynamic (MHD) nanofluid flow that occurred on a flexible sheet with variable thickness. Sharma et al. [16] examined the thermal and flow characteristics of magnetohydrodynamic (MHD) nanofluids near slender stretching sheets while analyzing dual effects of variable thickness alongside dissolution heat transfer models. Mabood et al. [17] conducted a numerical investigation on MHD boundary layer flow and heat transfer of nanofluids over a nonlinearly extending sheet while examining the effects between magnetic fields and nanofluid dynamics. The study by Krishnamurthy et al. [18] explored the process of slip flow and heat transfer during nanofluid melting under conditions of heat radiation and chemical reactions near a nonlinear extending sheet. Alkasasbeh [19] conducted a numerical study to analyze heat transfer in Casson hybrid nanofluid flowing near a vertical extending sheet under magnetic field influence. The study by Khan et al. [20] explored heat and mass transfer behavior of Williamson nanofluids under slanted Lorentz force acting on a nonlinear extending sheet. Wei-Miao et al. [21] expressed the effects of joule heating and electromagnetic power about Williamson nanofluid flows over a surface with changing thickness. Basit et al. [22] analyzed MHD hybrid nanofluid flows past an exponentially stretching sheet under thermal radiation and viscous dissipation conditions. Jain et al. [23] simulated a numerical model to understand how Williamson hybrid nanofluid (CuO / CNTs – water) behaves through permeable surfaces during extension or contraction under combined convective boundary conditions. Muhammed et al. [24] conducted numerical investigations into dissipative hybrid nanofluid flow over surfaces with uneven thickness which enabled melting heat transfer analysis. Recently Narmatha et al. [25] evaluated the magnetohydrodynamic flow of gasoline oil-based hybrid nanofluid with SWCNTs and Ag nanoparticles across non-uniform stretching surface. The current research investigates heat and mass transfer processes in the presence of melting conditions in the magnetohydrodynamic flows of hybrid nanofluids across thin stretching sheet.

2.MATHEMATICAL FORMULATION:

This study examines the flow dynamics of a hybrid nanofluid containing SWCNTs, *Ag* nanoparticles and gasoline oil over a slender stretching sheet. The sheet is stretched along the x −direction in a cartesian coordinate system (x, y) with a velocity profile expressed as $U_w = U_0(x + b)^m$, where $U_w$is the stretching velocity, U_0 is a constant, b is a scaling factor and m is an index behavior. The y – direction is taken normal to the surface of the sheet. This situation exhibits a non-uniform thickness that changes along the $x-$ direction, described by the relation $y = b^*(x + b)^{\frac{1-m}{2}}$ indicating varying thicknesses in x- direction. Here b^* denotes the thickness parameter and the exponent ensures a variable thickness profile dependent on the stretching parameter m.

Governing equations are

$$\frac{\partial u}{\partial x} + \frac{\partial v}{\partial y} = 0 \quad (1)$$

$$u\frac{\partial u}{\partial x}+v\frac{\partial u}{\partial y}=U_e\frac{dU_e}{dx}+\upsilon_{hnf}\frac{\partial^2 u}{\partial y^2}-\frac{\sigma B_0^2}{\rho_{hnf}}(U-U_e) \quad (2)$$

$$u\frac{\partial T}{\partial x}+v\frac{\partial T}{\partial y}=\alpha_{hnf}\frac{\partial^2 T}{\partial y^2}+\frac{\upsilon_{hnf}}{(\rho C_p)_{hnf}}\left(\frac{\partial u}{\partial y}\right)^2 \quad (3)$$

$$u\frac{\partial C}{\partial x}+v\frac{\partial C}{\partial y}=D_{B_{hnf}}\frac{\partial^2 C}{\partial y^2}+D_{T_{hnf}}\frac{\partial^2 T}{\partial y^2} \quad (4)$$

The initial and boundary conditions imposed on (1) - (4) are,

$$u=U_w(x)=U_0(x+b)^m, v=0, T=T_m, C=\ C_m \text{at } y=b^*(x+b)^{\frac{1-m}{2}}$$
$$u\to U_e(x)=U_\infty(x+b)^m, T\to T_\infty, C\to C_\infty \text{ at } y\to\infty \quad (5)$$

Melting heat conditions are exposed as;

$$k_{hnf}\left(\frac{\partial T}{\partial y}\right)_{y=b^*(x+b)^{\frac{1-m}{2}}}=\rho_{hnf}[\beta+C_s(T_m-T_0)]v_{y=b^*(x+b)^{\frac{1-m}{2}}} \quad (6)$$

Table 1. Thermophysical properties of nanoparticles by Mohammed et al. [24]

Nanoparticle/Thermophysical properties	$\rho\left(\frac{kg}{m^3}\right)$	$k\left(\frac{W}{mK}\right)$	$C_p\left(\frac{J}{kgK}\right)$	**Pr**
SWCNTs	1600	3000	796	-
Ag	10490	235	429	-
Gasoline oil	750	0.114	425	9.4

We adopt the following similarity transformations,

$$\eta=\sqrt{\frac{m+1}{2\upsilon_f}U_0(x+b)^{m-1}}.y,\ \psi=\sqrt{\frac{2\upsilon_f}{m+1}U_0(x+b)^{m+1}}f^*(\eta),\ \theta^*(\eta)=\frac{T-T_m}{T_\infty-T_m}, \Phi^*(\eta)=\frac{C-C_m}{C_\infty-C_m}$$

$$u=U_0(x+b)^m f^{*'}(\eta),\ \ v=-\sqrt{\frac{(m+1)\upsilon_f}{2}U_0(x+b)^{m-1}}\left(f^*(\eta)+\eta f^{*'}(\eta)\frac{m-1}{m+1}\right) \quad (7)$$

where ψ denotes the stream function, mathematically expressed as

$$u=\frac{\partial\psi}{\partial y}, v=-\frac{\partial\psi}{\partial x} \quad (8)$$

By applying the above similarity transformations, the equations (1)-(4) are simplified to

$$\frac{A_{11}}{(1-\varphi_1)^{2.5}(1-\varphi_2)^{2.5}} f^{*'''} + f^* f^{*''} + \frac{2m}{m+1}(A^2 - f^{*'^2}) - \frac{2}{m+1}\frac{Ha^2}{1+\lambda^2}(f^{*'} - A) = 0 \quad (9)$$

$$\frac{k_{hnf}}{k_f}\theta^{*''} + \frac{\Pr Ec}{(1-\varphi_1)^{2.5}(1-\varphi_2)^{2.5}} f^{*''^2} + B_{11} Pr \theta^{*'} f^* = 0 \quad (10)$$

$$\Phi^{*''} + Le\Phi^{*'} f^* + \frac{N_t}{N_b}\theta^{*''} = 0 \quad (11)$$

The corresponding boundary conditions are

$$f^{*'}(\alpha) = 1, \theta^*(\alpha) = 0, \frac{k_{hnf}}{k_f} M\theta^{*'}(\alpha) + A_{11}\left(Prf^*(\alpha) + \alpha\frac{m-1}{m+1}\right) = 0, \Phi^*(\alpha) = 0 \; at$$

$$\alpha = b^*\sqrt{\frac{m+1}{2\upsilon_f}U_0}$$

$$f^{*'}(\infty) \to A, \theta^*(\infty) \to 1, \Phi^*(\infty) \to 1 \text{ as } \alpha \to \infty. \quad (12)$$

where

$$A_{11} = \frac{1}{(1-\varphi_2)\left((1-\varphi_1)+\varphi_1\frac{\rho_{s1}}{\rho_f}\right)+\varphi_2\frac{\rho_{s2}}{\rho_f}} \quad (13)$$

$$B_{11} = \left((1-\varphi_2)\left((1-\varphi_1)C_{pf} + \varphi_1\frac{(\rho C_p)_{s2}}{\rho_f}\right)\right) + \varphi_2\frac{(\rho C_p)_{s1}}{\rho_f} \quad (14)$$

Here prime denotes differentiation and Wall thickness is $\alpha = b^*\sqrt{\frac{m+1}{2\upsilon_f}U_0}$.

Here we define $f^*(\eta) = f(\eta - \alpha) = f(\xi), \theta^*(\eta) = \theta(\eta - \alpha) = \theta(\xi), \; \Phi^*(\eta) = \Phi(\eta - \alpha) = \Phi(\xi)$. Hence equations (8) - (10) become

$$\frac{A_{11}}{(1-\varphi_1)^{2.5}(1-\varphi_2)^{2.5}} f''' + ff'' + \frac{2m}{m+1}(A^2 - f'^2) + \frac{2}{m+1}Ha^2(f' - A) = 0 \quad (15)$$

$$\frac{k_{hnf}}{k_f}\theta'' + \frac{\Pr Ec}{(1-\varphi_1)^{2.5}(1-\varphi_2)^{2.5}} f''^2 + B_{11} Pr\theta' f = 0 \quad (16)$$

$$\Phi'' + Le\Phi' f + \frac{N_t}{N_b}\theta'' = 0 \quad (17)$$

Boundary conditions are

$$f'(0) = 1, \theta(0) = 0, \frac{k_{hnf}}{k_f} M\theta'(0) + A_{11}\left(Prf(0) + \alpha\frac{m-1}{m+1}\right) = 0, \Phi(0) = 0$$

$f'(\infty) \to A, \theta(\infty) \to 1, \Phi(\infty) \to 1$ when $\xi \to \infty$

(18)

The non-dimensional parameters involved are

$$A = \frac{U_\infty}{U_0}, \alpha = b^* \sqrt{\frac{m+1}{2\upsilon_f} U_0}, Pr = \frac{\mu C_p}{k}, Ec = \frac{U_0^2 (x+b)^{2m}}{(T_\infty - T_m) C_{p_f}}, M = \frac{C_{p_f}(T_\infty - T_m)}{\lambda + C_s(T_m - T_0)},$$

$$Ha^2 = \frac{\sigma B_0^2 (x+b)^{m-1}}{\rho_f U_0}, \; Le = \frac{\gamma_f}{D_B}, N_t = \frac{D_T(T_\infty - T_m)}{\gamma_{hnf}}, N_b = \frac{D_B(C_\infty - C_m)}{\gamma_{hnf}} \quad (19)$$

3.MATHEMATICAL REPRESENTATION OF NONDIMENSIONALESS PARAMETERS

Skin friction coefficient(C_f) is defined as

$$C_f = \frac{\tau_w}{\rho_f U_w^2}$$

(20)

where $\tau_w = \mu_{hnf}\left(\frac{\partial u}{\partial y}\right)_{y=b^*\sqrt{\frac{m+1}{2\upsilon_f}U_0}}$

(21)

Local Nusselt number(Nu_x) is defined as

$$Nu_x = \frac{(x+b)q_w}{k(T_\infty - T_m)}$$

(22)

where $q_w = -k_{hnf}\left(\frac{\partial T}{\partial y}\right)_{y=b^*\sqrt{\frac{m+1}{2\upsilon_f}U_0}}$

(23) Local Sherwood number(Sh_x) is defined as

$$Sh_x = \frac{(x+b)q_m}{D_B(C_\infty - C_m)}$$

(24)

where $q_m = -D_{B\,hnf}\left(\frac{\partial C}{\partial y}\right)_{y=b^*\sqrt{\frac{m+1}{2\upsilon_f}U_0}}$

(25)

Substitute equations (21), (23) and (25) in equations (20),(22) and (24) we get,

$$C_f\sqrt{Re_x} = \frac{1}{(1-\varphi_1)^{2.5}(1-\varphi_2)^{2.5}}\sqrt{\frac{m+1}{2}} f''(0)$$

(26)

$$\frac{Nu_x}{\sqrt{Re_x}} = -\frac{k_{hnf}}{k_f}\sqrt{\frac{m+1}{2}}\theta'(0)$$

(27)

$$\frac{Sh_x}{\sqrt{Re_x}} = -\sqrt{\frac{m+1}{2}}\Phi'(0) \quad (28)$$

where the local Reynolds number is defined as $Re_x = \frac{U_0(x+b)^{m+1}}{\upsilon_f}$.

4.FRAMEWORK FOR NANOFLUID AND HYBRID NANOFLUID

For nanofluid we obtained [16];

$$\mu_{nf} = \frac{\mu_f}{(1-\varphi_1)^{2.5}}$$

$$\upsilon_{nf} = \frac{\mu_{nf}}{\rho_{nf}}$$

$$(\rho C_p)_{nf} = (1-\varphi_1)(\rho C_p)_f + \varphi_1(\rho C_p)_{s1}$$

$$\rho_{nf} = (1-\varphi_1)\rho_f + \varphi_1\rho_{s1}$$

$$\frac{k_{nf}}{k_f} = \frac{k_{s1} + (n-1)k_f - (n-1)\varphi_1(k_f - k_{s1})}{k_{s1} + (n-1)k_f + \varphi_1(k_f - k_{s1})}$$

For hybrid nanofluid, we have:

$$\mu_{hnf} = \frac{\mu_f}{(1-\varphi_1)^{2.5}(1-\varphi_2)^{2.5}}$$

$$(\rho C_p)_{hnf} = (1-\varphi_2)\left((1-\varphi_1)(\rho C_p)_f + \varphi_1(\rho C_p)_{s1}\right) + \varphi_2(\rho C_p)_{s2}$$

$$\rho_{hnf} = (1-\varphi_2)\left((1-\varphi_1)\rho_f + \varphi_1\rho_{s1}\right) + \varphi_2\rho_{s2}$$

$$\frac{k_{hnf}}{k_f} = \frac{k_{s2} + (n-1)k_f - (n-1)\varphi_2(k_f - k_{s2})}{k_{s2} + (n-1)k_f + \varphi_2(k_f - k_{s2})}$$

$$\frac{k_{bf}}{k_f} = \frac{k_{s1} + (n-1)k_f - (n-1)\varphi_1(k_f - k_{s1})}{k_{s1} + (n-1)k_f + \varphi_1(k_f - k_{s1})}$$

5.NUMERICAL RESULTS

The flow expressions are transformed into ODEs and subsequently solved utilizing the shooting method that involve these computational steps.

$$f_1 = f\,; f_2 = f_1' = f'\,;\ f_3 = f_2' = f'';$$

$$f_4 = f_3' = f''' = -\frac{(1-\varphi_1)^{2.5}(1-\varphi_2)^{2.5}}{A_{11}}\left(f_1 f_3 + \frac{2m}{m+1}(A^2 - {f_2}^2) - \frac{2Ha^2}{m+1}(f_2 - A)\right);$$

$$f_5 = f_4' = \theta'\,;\ f_6 = f_5' = \theta'' = \frac{1}{\left(\frac{k_{hnf}}{k_f}\right)}\left(-B_{11}Pr f_1 f_6 - \frac{\Pr Ec}{(1-\varphi_1)^{2.5}(1-\varphi_2)^{2.5}}(f_3)^2\right);$$

$$f_7 = f_6' = \Phi'\,;\ f_8 = f_7' = \Phi'' = -Le\, f_7 f_1 - \frac{N_t}{N_b} f_6.$$

$$f_2(0) = 1, f_5(0) = 0, \frac{k_{hnf}}{k_f} M f_6(0) + A_{11}\left(Pr f_1(0) + \alpha \frac{m-1}{m+1}\right) = 0, f_7(0) = 0$$

$$f_2(\infty) \to A, f_5(\infty) \to 1, f_7(\infty) \to 1 \text{ as } \xi \to \infty.$$

6. GRAPHS:

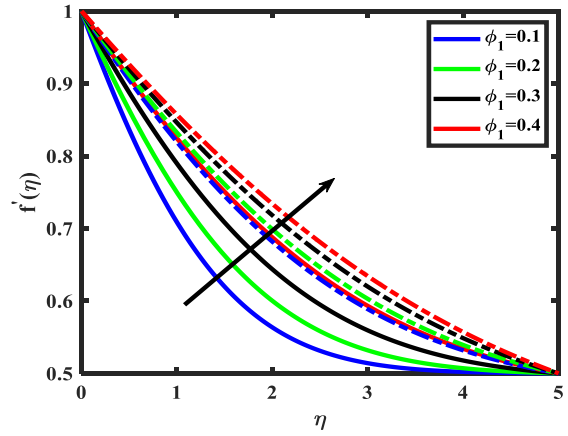

Plot 1. Modulation of φ_1 on $f'(\eta)$ at Ha = 0.

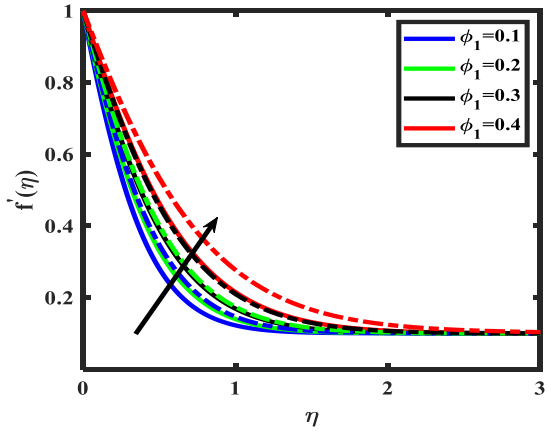

Plot 2. Modulation of φ_1 on $f'(\eta)$.

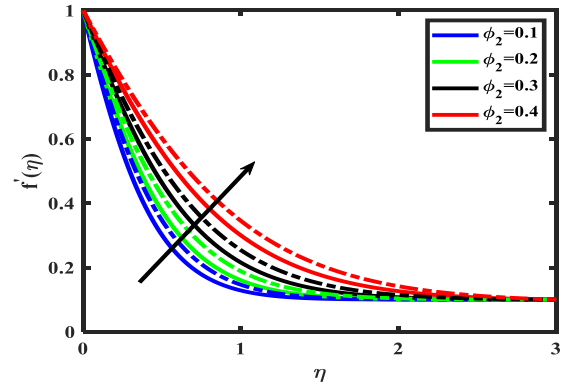

Plot 3. Modulation of φ_2 on $f'(\eta)$.

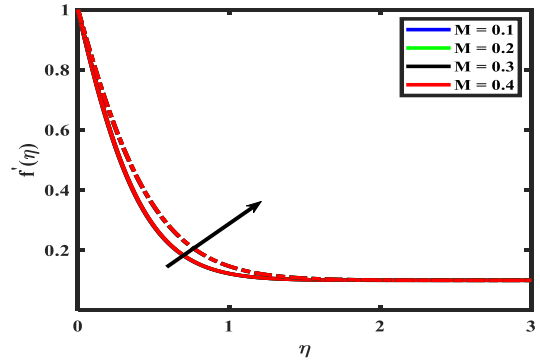

Plot 4 . Modulation of M on $f'(\eta)$.

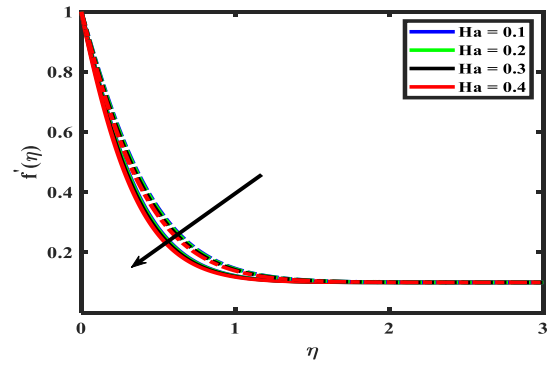

Plot 5. Modulation of Ha on $f'(\eta)$.

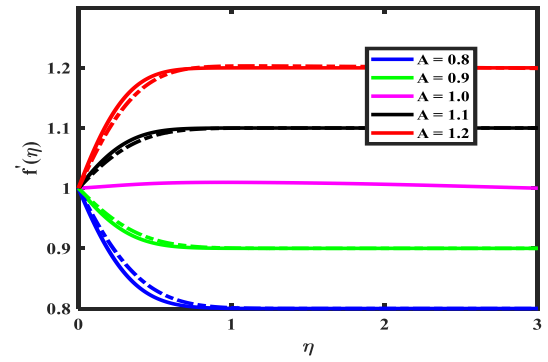

Plot 6. Modulation of A on $f'(\eta)$.

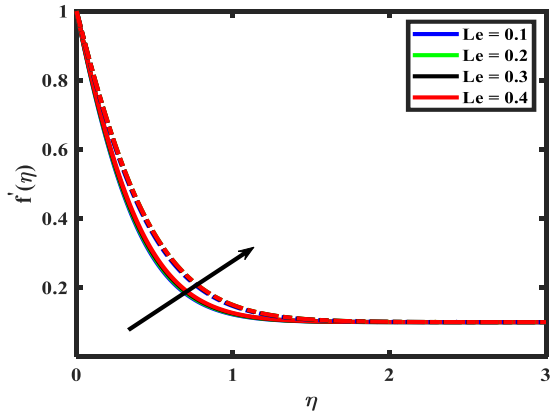

Plot 7. Behavior of Le on $f'(\eta)$.

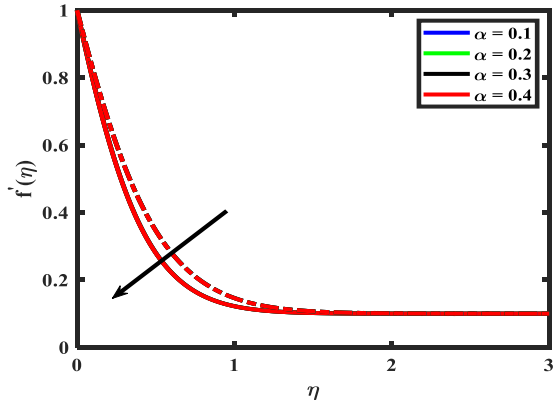

Plot 8. Behavior of α on $f'(\eta)$.

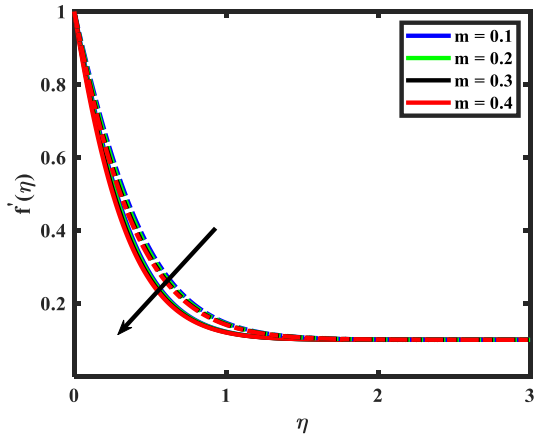

Plot 9. Modulation of m on $f'(\eta)$.

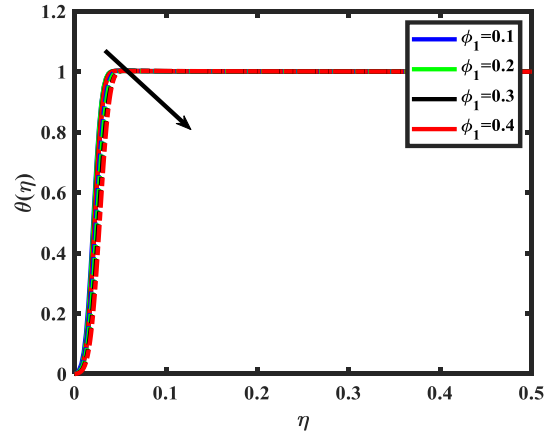

Plot 10. Modulation of φ_1 on $\theta(\eta)$.

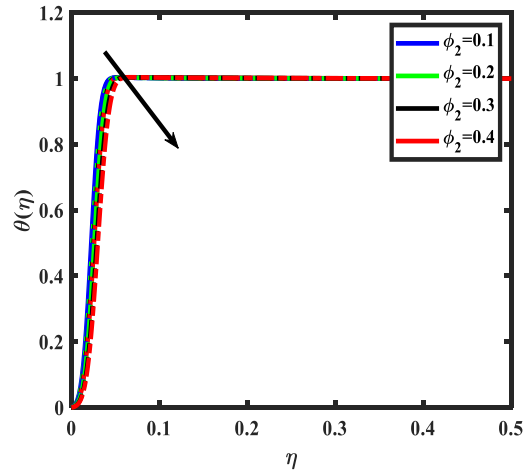

Plot 11. Modulation of φ_2 on $\theta(\eta)$.

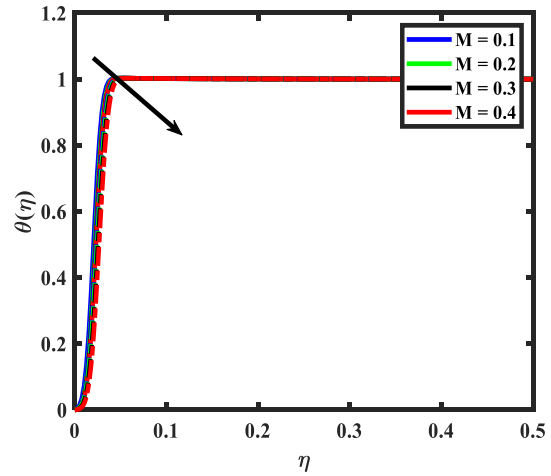

Plot 12. Modulation of M on $\theta(\eta)$.

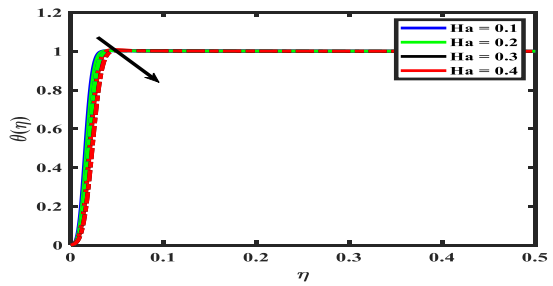

Plot 13. Modulation of Ha on $\theta(\eta)$.

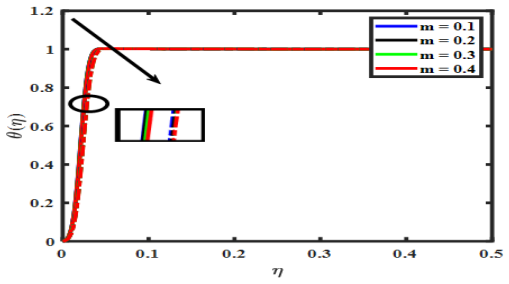

Plot 14. Modulation of m on $\theta(\eta)$.

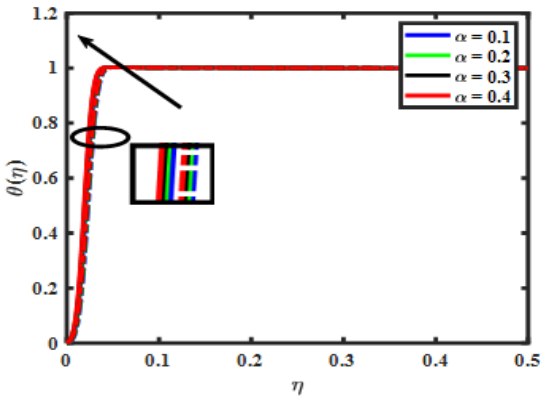

Plot 15. Modulation of α on $\theta(\eta)$.

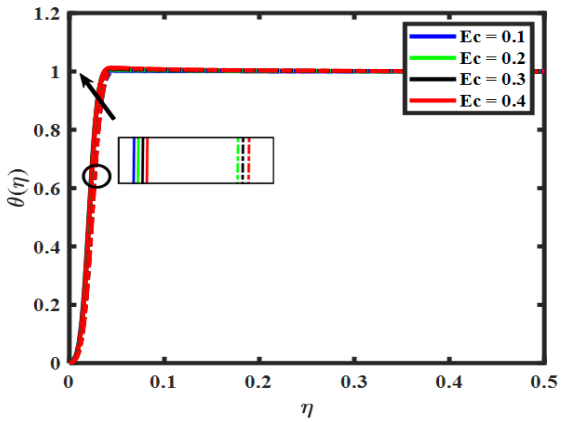

Plot 16. Modulation of EC on $\theta(\eta)$.

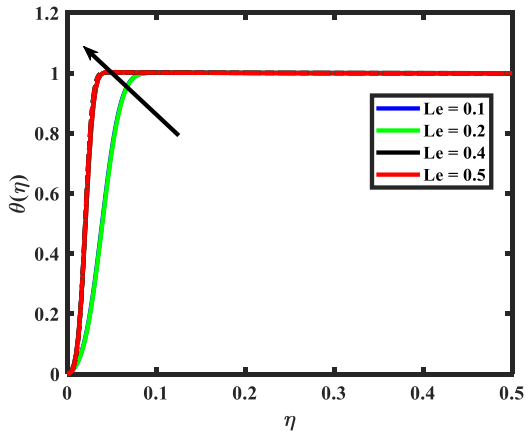

Plot 17. Modulation of Le on $\theta(\eta)$.

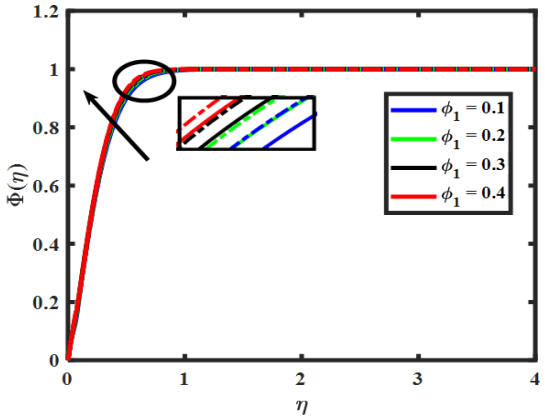

Plot 18. Modulation of φ_1 on $\Phi(\eta)$.

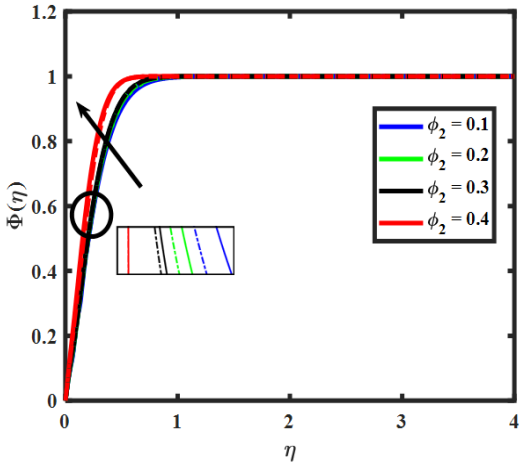

Plot 19. Modulation of φ_1 on $\Phi(\eta)$.

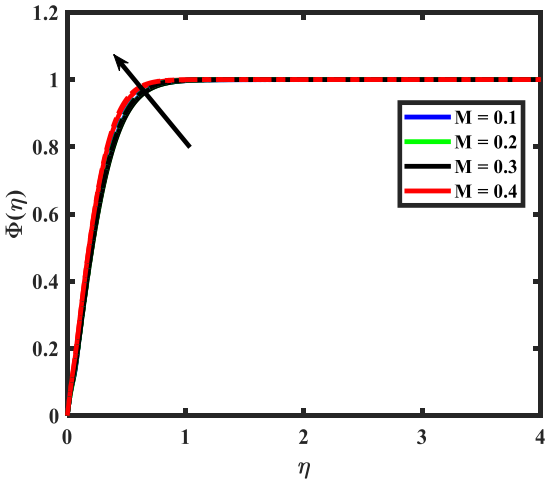

Plot 20. Modulation of M on $\Phi(\eta)$.

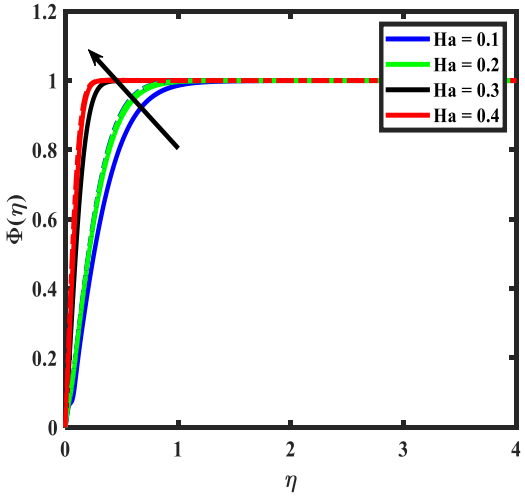

21. Modulation of Ha on $\Phi(\eta)$.

Plot

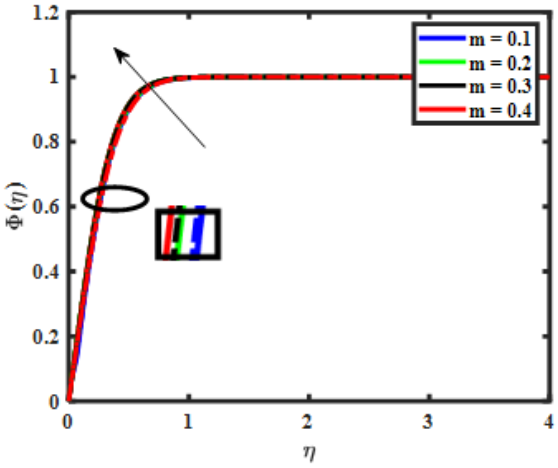

Plot 22. Modulation of m on $\Phi(\eta)$.

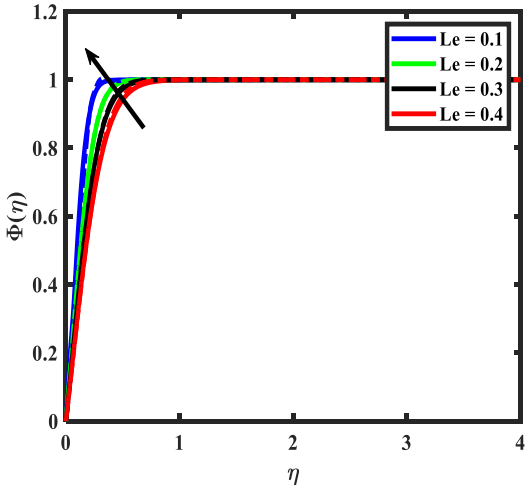

Plot 23. Modulation of Le on $\Phi(\eta)$.

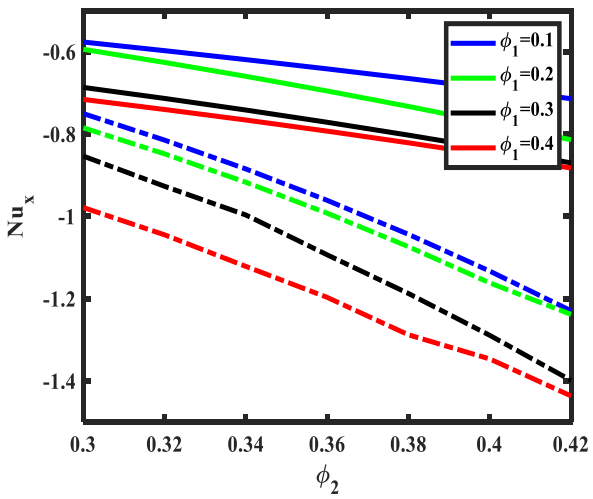

Plot 24. Modulation of $\varphi_1$and φ_2 on Nu_x.

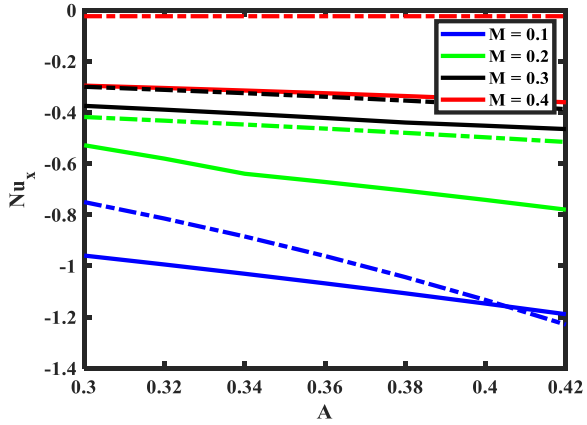

Plot 25. Modulation of M and A on Nu_x.

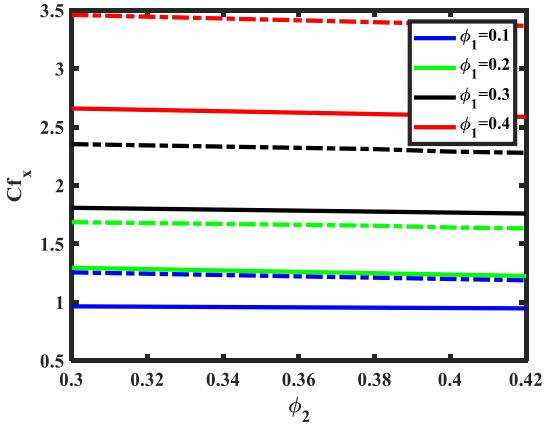

Plot 26. Modulation of $\varphi_1$and φ_2 on C_{fx}.

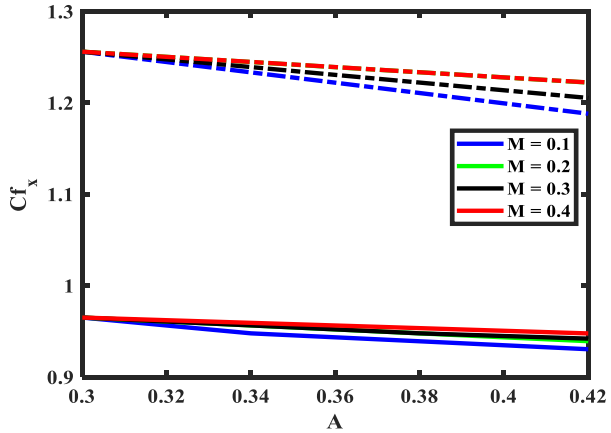

Plot 27. Modulation of M and A on C_{fx}.

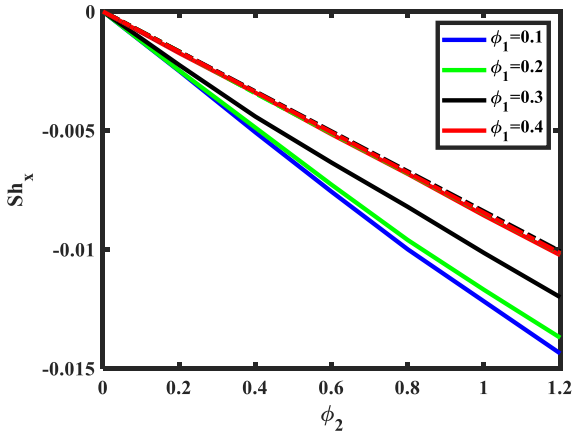

Plot 28. Modulation of $\varphi_1$and φ_2 on Sh_x.

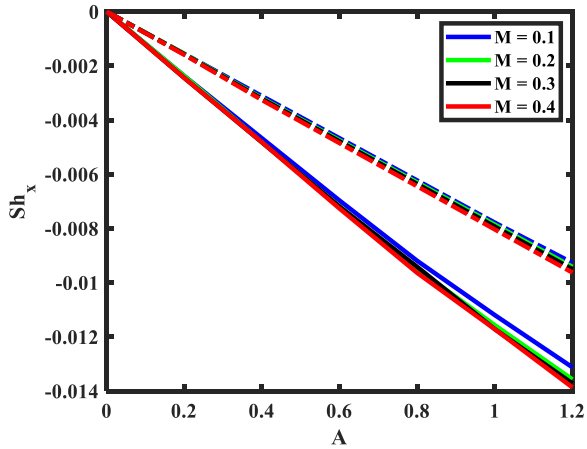

Plot 29. Modulation of M and A on Sh_x.

7. RESULTS AND DISCUSSION:

In this research, the shooting method is used to analyse the model represented by equations (15)-(17) along with the respective boundary constraints in equation (18) for varying parameter values.

This work investigates how various flow parameters affect dimensionless velocity, temperature and concentration distributions in addition to skin friction and the rates of heat and mass transfer.

Plot 1 illustrates the impact of volume fraction of SWCNTs on $f'(\eta)$ at vanishing Hartmann number. It shows that $f'(\eta)$ increases with increments in the volume fraction when compared to the earlier study of Muhammed *et al*. [24], These results show a strong consistency with earlier studies. The volume fraction of φ_1(SWCNTS) on the dimensionless velocity profile $f'(\eta)$ as shown in Plot 2, shows an apparent rise with the higher values throughout the boundary layer as $\varphi_1$rises from$[0.1, 0.4]$. Plot 3 depicts that as volume fraction of φ_2(Ag) increases, the velocity profile $f'(\eta)$. Plot 4 reveals that increasing melting heat parameter M enhances the velocity profile $f'(\eta)$, Higher melting heat leads to increased thermal energy absorption near the surface which facilitates the melting process. The velocity profile decreases with rising Hartmann number (Ha) as shown in Plot 5. The magnetic field generates a Lorentz force that opposes the flow of fluid which causes the velocity profile to decrease. The influence of parameter A on the velocity profile $f'(\eta)$ is shown in Plot 6. It illustrates about how it significantly influences the flow motion and boundary layering. The graph shows that when $A > 1$, the boundary layer becomes thicker due to the acceleration of the velocity profile. Conversely, the boundary layer thins when A < 1, indicating restrained flow near the surface. At $A = 1$, the absence of a boundary layer signifies a critical transitional state in the fluid flow. The impact of Lewis number (Le), on $f'(\eta)$ fixed as $[0.1, 0.4]$ is illustrated in Plot 7. The heat transfer rate becomes more prominent, in improving the characteristics of thermal boundary layer and reduces viscous resistance leading to higher velocity gradients near the surface of the boundary layer.

The velocity profile $f'(\eta)$, shows faster decay with increasing values of α, indicating stronger restriction of fluid movement near the surface as demonstrated in Plot 8. Plot 9 represents the influence of index behaviour parameter m on $f'(\eta)$. It can be noticed that the velocity profile declines faster with increasing index parameter m, highlighting an accelerated decay in fluid motion. Plot 10 exhibits the effects of volume fraction of φ_1, on temperature profile $\theta(\eta)$. Temperature profile minimizes with increasing values of φ_1 from 0.1 to 0.4. Plot 11 presents the influence of volume fraction of $\varphi_2$on $\theta(\eta)$. The thermal conductivity improves alongside heat transfer efficiency as the parameter φ_2 rises from $[0.1, 0.4]$, because the temperature profile $\theta(\eta)$ decreases in this range. The temperature distribution $\theta(\eta)$ decreases according to Plot 12 because increasing the melting parameter M reduces $\theta(\eta)$. The rising values of Hartmann number (Ha) from $[0.1, 0.4]$ result in decrease of $\theta(\eta)$ as evident in Plot 13. The Lorentz force acts to suppress heat transfer thus creating a thicker thermal boundary layer.

The temperature profile $\theta(\eta)$ decreases according to Plot 14 when the index behaviour parameter m grows from [0.1,0.4]. The wall thickness parameter α affects $\theta(\eta)$ according to Plot 15 where temperature rises when α values increase from [0.1,0.4]. The surface heat retention increases because of which thermal energy spreads more effectively throughout the fluid. The temperature profile $\theta(\eta)$ grows higher as the Eckert number (Ec) ranges from [0.1,0.4] in Plot 16 because kinetic energy transforms into thermal energy. Plot 17 demonstrates that the Lewis number increase produces raised values of $\theta(\eta)$ while maintaining its constant range. A higher nanoparticle volume fraction from [0.1,0.4] produces stronger concentration profile $\Phi(\eta)$ in Plot 18 due to better microparticle interaction and better mass transportation. A higher volume fraction φ_2 as per Plot 19 results in increased concentration profile $\Phi(\eta)$ which leads to better distribution uniformity along with superior system performance. The concentration profile $\Phi(\eta)$ shows a steady rise during the increase of M from [0.1,0.4] in Plot 20, since improved melting heat increases mass diffusion near the surface and throughout the fluid solution. The increase in Hartmann number elevates $\Phi(\eta)$ values because

intensifying magnetic effects minimize fluid movement and accelerate mass diffusion which strengthens the concentration boundary layer stability as shown in Plot 21. The graphical analysis in Plot 22 shows that increasing m values in index produces an elevation of $\Phi(\eta)$ which indicates better fluid behaviour and enhanced mass transport capabilities. Studies represented in Plot 23 demonstrate that increasing the Lewis number enhances $\Phi(\eta)$. Higher concentration gradients result in improving mass transfer efficiency inside the boundary layer.

As illustrated in Plots 1-23, the hybrid nanofluid demonstrates superior efficiency over the conventional nanofluid. The influence of φ_1, φ_2, M and A respectively on the rate of heat transfer Nu_x, wall shear stress C_{f_x} and mass transfer Sh_x are depicted respectively in Plots 24 & 25, 26&27 and 28&29. It can be observed that skin friction and mass transfer rate increase with higher values of φ_1, φ_2, M and A. Conversely, the heat transfer rate declines as these parameters rise.

Across all cases, the hybrid nanofluid exhibits more pronounced enhancements in thermal and fluid dynamic performance compared to the standard nanofluid.

8. SUMMARY OF SIGNIFICANT RESULTS

The main purpose of this study is to emphasize on melting heat on magnetohydrodynamic, heat and mass transfer systems using SWCNTs mixed with Ag as a hybrid nanoparticle and Gasoline as the base fluid.

The results of our study are

- The flow gets accelerated with increases in the volume fraction of SWCNTs (φ_1), volume fraction of Ag (φ_2), melting heat (M), velocity ratio parameter (A) and Lewis number (Le).
- The flow velocity $f'(\eta)$ decelerates with increase in the index behaviour (m), Hartmann number (Ha) and wall thickness parameter (α).
- The temperature profile θ(η) diminishes with increments in the volume fraction of SWCNTs (φ_1), the volume fraction of Ag (φ_2), melting heat (M), Hartmann number (Ha), and index behaviour (m).
- The temperature profile increases with enhancements in the Eckert number (Ec), wall thickness parameter (α), and Lewis number (Le).
- Concentration profile $\Phi(\eta)$ decreases with higher values of the volume fraction of SWCNTs (φ_1), volume fraction of Ag (φ_2) and melting heat (M).
- Flow of concentration profile $\Phi(\eta)$ is maximized with increments in Hartmann number (Ha), index behavior (m), and Lewis number (Le).
- Wall shear stress coefficient is analyzed for various parameters such as of φ_1, φ_2, A & M. Results reveal that shear stress increases with higher values of φ_1 and $\varphi_2$and also it increases with the values of M and A.
- Analyses of the Nusselt number focused on the examination of parameters φ_1, φ_2, A & M. The research findings show that elevating the values of φ_1 and φ_2 results in reduced Nusselt number performance. The Nusselt number rises progressively alongside increasing the values M and A.

- Sherwood number is analysed across parameters such as of φ_1, φ_2, A & M. The results indicate that the Sherwood number rises with the increasing values of φ_1 and $\varphi_2$while it decays with increasing values of M and A.
- In particular, the above mentioned results show that the performance of hybrid nanofluid is better when compared to the nanofluid.

9. NOMENCLATURE

u, v	velocity components
α_f	thermal diffusivity (gasoline oil)
μ_f	dynamic viscosity (gasoline oil)
ρ_f	density (gasoline oil)
x, y	cartesian coordinates
k_f	thermal conductivity (gasoline oil)
A	velocity ratio parameter
υ_f	kinematic viscosity
θ	dimensionless temperature
Φ	dimensionless Concentration
f	non-dimensional velocity
T_w	wall temperature
m	behavior index parameter about flow
q_w	wall heat flux
φ_1	volume fraction (SWCNTs)
φ_2	volume fraction (Ag)
$(C_p)_f$	specific heat (gasoline oil)
M	melting parameter
Pr	Prantl Number
α	wall thickness parameter
U_0, U_∞	arbitrary constant
C_s	heat capacity (solid surface)
U_e	free stream velocity
T_∞	ambient temperature
C_∞	ambient concentration
τ_w	wall shear stress

U_w stretching velocity

q_m wall mass flux

β latent heat

Ec Eckert number

T_m surface temperature

C_m surface concentration

Le Lewis number

N_t Thermophoresis

N_b Brownian motion

k_{s1} thermal conductivity (SWCNTs)

n nanoparticle shape

k_{s2} thermal conductivity (Ag)

CNTs carbon nanotubes

SWCNTs single valued carbon nanotubes

Ag Silver

C_8H_{18} Gasoline oil

For nanofluid

α_{nf} thermal diffusivity

μ_{nf} dynamic viscosity

υ_{nf} kinematic viscosity

k_{nf} thermal conductivity

ρ_{nf} density

$(C_p)_{nf}$ specific heat

For hybrid nanofluid

α_{hnf} thermal diffusivity

$(C_p)_{hnf}$ Specific heat

k_{hnf} thermal conductivity

μ_{hnf} dynamic viscosity

υ_{hnf} kinematic viscosity

ρ_{hnf} density

$D_{B_{hnf}}$ Brownian diffusion

$D_{T_{hnf}}$ Thermophoresis diffusion

REFERENCES

[1] Choi S U S, and Jeffrey Eastman A. "Enhancing thermal conductivity of fluids with nanoparticles", *Report No. ANL/MSD/CP-84938; CONF-951135-29, International mechanical engineering congress and exhibition, San Francisco, CA (United States).,* **1995**, 12 – 17.

[2] Vajravelu K. "Viscous flow over a nonlinearly stretching sheet", *Appl. Math. Comput.*, **2001**,124, 281–288.

[3] Fang T, Zhang J and Zhong Y. "Boundary layer flow over a stretching sheet with variable thickness", *Appl Math Comput.,* **2012**, 218, 7241–52 (2012).

[4] Ali, Aamir, S. Saleem, Sana Mumraiz, Anber Saleem, M. Awais, and D. N. Khan Marwat. "Investigation on TiO2– Cu/H2O hybrid nanofluid with slip conditions in MHD peristaltic flow of Jeffrey material", *Journal of Thermal Analysis and Calorimetry.*, **2021**,143(3), 1985-1996.

[5] Jahan S, Sakidin H, Nazar R, Pop I. "Flow and heat transfer past a permeable nonlinearly stretching/shrinking sheet in a nanofluid: A revised model with stability analysis", *J Mol Liq*, **2017**, 233, 211–221.

[6] Mukhopadhyay, S. "MHD boundary layer flow and heat transfer over an exponentially stretching sheet embedded in a thermally stratified medium", *Alexandria Engineering Journal,* **2013**,52(3), 259-265.

[7] Roberts L, "On the melting of a semi-infinite body of ice placed in a hot stream of air", *J. Fluid Mech.*, **1958**, 4, 505–528.

[8] Gireesha B J, Mahanthesh B, Shivakumara I S and Eshwarappa K M, "Melting heat transfer in boundary layer stagnation-point flow of nanofluid toward a stretching sheet with induced magnetic field", *Eng. Sci. Technol.*, **2016**, 19 (1), 313–321.

[9] Gireesha B., Venkatesh, P., Shashikumar, N. and Prasannakumara B, "Boundary layer flow of dusty fluid over a radiating stretching surface embedded in a thermally stratified porous medium in the presence of uniform heat source", *Nonlinear Engineering,* **2017**, 6(1), 31-41.

[10] Tasawar Hayat., Meraj Mustafa., Zahid Iqbal., and Alsaedi A., "Stagnation-point flow of couple stress fluid with melting heat transfer", *Applied Mathematics and Mechanics - english Edition,* **2013**, 34(2), 167-176.

[11] Khilap Singh. and Manoj Kumar, "Melting and heat absorption effects in boundary layer stagnation-point flow towards a stretching sheet in a micropolar fluid", *Ain Shams Engineering Journal,* **2018**, 9(4), 861-868.

[12] Hayat T, Muhammad K, Farooq and Alsaedi A, "Melting heat transfer in stagnation point flow of carbon nanotubes towards variable thickness surface", *AIP Adv.*, 2016, 6,015214(1-9).

[13] M. Turkyilmazoglu, "Natural convective flow of nanofluids past a radiative and impulsive vertical plate", *J. Aerosp. Eng.*, **2016**, 29, 1–8 (2016).

[14] Khader, M. M., and Megahed, A. M, "Numerical solution for boundary layer flow due to a nonlinearly stretching sheet with variable thickness and slip velocity", *The European physical journal plus,* **2013**, 128, 1-7.

[15] Prasad K V, Vajravelu K, Vaidya H and Van Gorder R A, "MHD flow and heat transfer in a nanofluid over a slender elastic sheet with variable thickness", *Results Phys,* **2017**, 7,1462–1474.

[16] Sharma, R. P., Acharya, N., and Das, K. "On the impact of variable thickness and melting transfer of heat on magnetohydrodynamics nanofluid flow past a slender stretching sheet"*, Indian journal of geomarine sciences*, **2020**, 49(4), 641-648.

[17] Mabood, F., Khan, W.A and Ismail, A.I.M., "MHD boundary layer flow and heat transfer of nanofluids over a nonlinear stretching sheet: a numerical study", *J. Magn. Magn. Mater.*, **2015**, 374,569–576.

[18] Krishnamurthy M.R., Gireesha, B.J. and Gorla, R.S.R. "Thermal radiation and chemical reaction effects on boundary layer slip flow and melting heat transfer of nanofluid induced by nonlinearly stretching sheet"*, Nonlinear Eng.* **2016**, 5, 147–159.

[19] Alkasasbeh H. "Numerical solution of heat transfer flow of casson hybrid nanofluid over vertical stretching sheet with magnetic field effect"*, CFD Letters*, **2022**, 14(3), 39-52.

[20] Khan M., Malik M. Y., Salahuddin T., and Hussian A, "Heat and mass transfer of Williamson nanofluid flow yield by an inclined Lorentz force over a nonlinear stretching sheet", *Results in physics*, **2018**, 8, 862-868.

[21] Wei-Miao Q., Fazal H., M IjazK., Sohail A, K., and Shahid F, "Modeling and analysis of magnetized nanomaterial Williamson towards a variable thicked surface subject to Joule heating and activation energy", *Journal of Magnetics*, **2021**, 26(2),146-155.

[22] Basit, A., Zahid, M., and Liśkiewicz, G. "Analysis of MHD hybrid nanofluid through an exponential stretching sheet with dissipation and radiation effects", *Authorea Preprints*, **2023**, 6, 1-25.

[23] Jain, R., Mehta, R., Bhatnagar, A., Ahmad, H., Khan, Z. A., and Ismail, G. M. "Numerical study of heat and mass transfer of Williamson hybrid nanofluid (CuO/CNT's-water) past a permeable stretching/shrinking surface with mixed convective boundary condition"*, Case Studies in Thermal Engineering,* **2024**, 59, 104313.

[24] Muhammad K, Hayat T, and Alsaedi A. "Numerical study for melting heat in dissipative flow of hybrid nanofluid over a variable thicken surface"*, International Communications in Heat and Mass Transfer,* **2021**, 121**,** 104805(1-10) (2021).

[25] Narmatha M, Rohith Roshan A and Sumathi K., "Numerical investigation of melting heat transfer in magnetohydrodynamic flow of hybrid nanofluid (SWCNTs + Ag + Gasoline) over a non-uniform stretching sheet", *Journal of Computational Analysis and Applications*., **2024**, 33(05), 884–897.